Polymer Chemistry

ROYAL SOCIETY OF CHEMISTRY

PAPER

View Article Online
View Journal | View Issue

Check for updates

Cite this: *Polym. Chem.*, 2024, **15**, 1726

Broad-spectrum lignin-based adhesives using thiol–silyl ether crosslinkers†

Yishayah Bension, Siteng Zhang, Tristan Menninger, Ting Ge * and Chuanbing Tang *

Received 8th December 2023,
Accepted 20th March 2024

DOI: 10.1039/d3py01355c

rsc.li/polymers

Lignin is a renewable feedstock that is abundant and inexpensive but still presents challenges for its valorization. In this work, we converted functionalized lignin into broad-spectrum adhesives using thiol–silyl ether crosslinkers. The curing behavior of adhesives was investigated *via* rheology of their resin forms. These materials exhibit good adhesion on diverse substrates, including wood, glass, steel, aluminium, carbon fiber, and different plastics, with the most adhesion strength in the range of 1–3 MPa. These adhesives were also explored for applications, ranging from wet conditions to different mechanically responsive materials. The mechanism of adhesion was further examined to understand the bonding process.

1. Introduction

Modern adhesives, such as epoxy resins or latex, offer high adhesion strength on a diverse range of substrates.[1–3] However, the feedstocks for the manufacturing of these materials are often fossil fuels that are increasingly unsustainable and undesirable for environments therefore greener adhesives are required.[4–6] To create a greener adhesive, lignin was examined as a potential feedstock. Lignin is a complex organic polymer found in the cell walls of many plants, making it one of the most abundant renewable resources on Earth. Lignin is produced in large quantities as a by-product of the paper and pulp industry, as well as in various other industries such as biofuels, chemicals, and materials.[7–9] Lignin is widely used as a source of sustainable materials due to its abundance, biodegradability, and unique chemical properties. Lignin is composed of three types of monolignols: *p*-coumaryl alcohol, coniferyl alcohol, and sinapyl alcohol, which are polymerized through radical reactions.[10] The abundance of hydroxyl moieties on lignin allows for further functionalization such as amination, oxidation, and polymerization.[11–16]

One of the functions of lignin in plants is to act as an adhesive between cellulose and hemicellulose components, making it an exemplary candidate for incorporation into synthetic adhesives.[17] Adhesives work by maximizing interactions between two substrates. Adhesive interactions may be divided into two components, nonbonding and bonding.[18,19] The strongest interactions are conventionally covalent linkages that form at the interface between a substrate and an adhesive.[20] Siloxanes or epoxy resins can form bonds between surfaces enhancing the adhesion significantly.[21] The other adhesive component is nonbonding interactions such as hydrogen bonding or supramolecular interactions.[22,23] While typically weaker, these forces can play an important role in underwater adhesion or polymer composites. Even with strong nonbonding and bonding components, it is very difficult for an adhesive to achieve strong interfacial adhesion across a wide variety of substrates.[24] Polar substrates such as wood often have porous surfaces making it difficult to apply an even layer of adhesive to promote strong interfacial contact between two substrates. Nonpolar surfaces such as polyethylene have lower surface energies due to the absence of polar groups making nonbonding and bonding interactions difficult to form.[25] Overall, synthetic adhesives must consider not only the chemistry of an adhesive but also the bonding and nonbonding interactions with the surface.

Much research into lignin-based adhesives has already been conducted. Lignin-glyoxal formulations utilizing Cannizzaro reaction show great promise as wood adhesives.[26,27] However, these materials do not show a broad substrate compatibility and can give off toxic byproducts such as formaldehyde. Other research focused on incorporating polymers to create a composite lignin adhesive.[28,29] These materials display enhanced adhesion at the cost of sustainability and often require difficult curing conditions. One promising route is the use of click chemistry to crosslink adhesives, thus enhancing the interfacial adhesion.[30,31] Epoxides are easily attacked by nucleophiles such as alcohols and amines

Department of Chemistry and Biochemistry, University of South Carolina, Columbia, South Carolina, 29208, USA. E-mail: tang4@mailbox.sc.edu, tingg@mailbox.sc.edu

† Electronic supplementary information (ESI) available. See DOI: https://doi.org/10.1039/d3py01355c

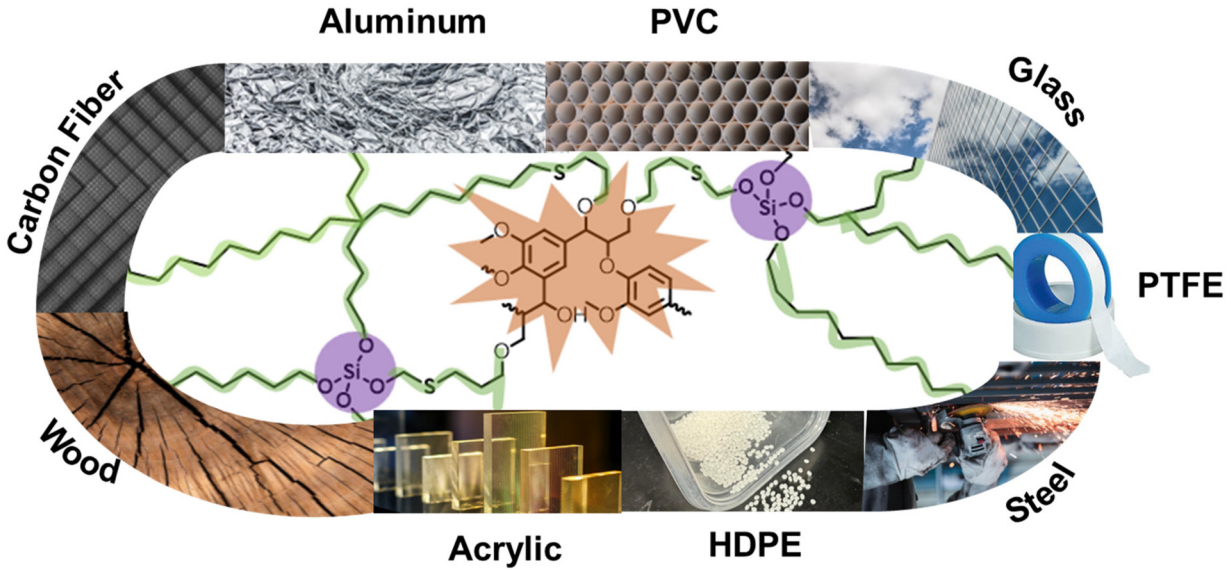

Fig. 1 Graphical representation of broad-spectrum lignin-based adhesives on diverse substrates using thiol–silyl ethers as crosslinkers *via* thiol–ene click chemistry.

via nucleophilic substitution. Many epoxy resins are excellent adhesive materials due to their efficient crosslinking, mild reaction conditions, and a wide variety of commercially available crosslinkers but are often manufactured from bisphenols, which pose safety hazards and environmental concerns.[32]

In this work, we explore click-type thiol–ene addition to prepare lignin-based adhesives (Fig. 1). Similar to epoxide substitution, thiol–ene reaction is atom-efficient, thermally initiated, and compatible with different crosslinkers. Previously, we explored thermosets of different thiol–silyl ethers as crosslinkers.[33] Herein, these thermosets were evaluated as adhesives and thermally cured on different substrates to assess adhesion strength. The mechanism of adhesion was computationally, experimentally, and rheologically explored.

2. Experimental

2.1 Materials

Organosolv lignin (Lignol Corporation, M_n = 1200 g mol^{-1}, $Đ$ = 4.4, hydroxyl value = 5.62 mmol g^{-1}), allyl bromide (99%, Alfa Aesar), sodium hydroxide (NaOH 99%, Fischer Scientific), 10-undecen-1-ol (98%, Sigma Aldrich), imidazole (99%, VWR), benzoin (98%, TCI), thioacetic acid (97%, Alfa Aesar), dichlorodiisopropylsilane (98%, TCI), tetrachlorosilane (98%, TCI), methanol (MeOH), dichloromethane (DCM), tetrahydrofuran (THF), and all other reagents were from commercial resources and used as received. Substrates were cut to specifications and ordered from SendCutSend LLC, USA (Reno NV).

2.1.1 Lignin allylation. A procedure was modified according to literature.[33,34] Unfractionated Lignin (5.5 g) was dissolved in THF (60 mL) and stirred until the solution was homogenous with a light brown color. Sodium hydroxide (5.5 g, 137.5 mmol) was then dissolved in deionized water (4 mL) and added to the lignin solution. The resulting mixture was stirred while allyl bromide (6.5 g, 53.7 mmol) was slowly added, and the temperature was set to 65 °C and the reaction was allowed to stir for 48 hours. Afterwards the reaction was quenched by adding 0.1 M HCl and the resulting precipitate was placed under a rotary evaporator to remove the solvent. The brown solid was washed with water and then dried under vacuum with a final dry weight of 7.13 g. The allylation was verified according to ^{1}H NMR and FTIR (Fig. S1 and S2†). The total conversion of hydroxyl groups to ally groups was calculated to be about 95% according to ^{31}P NMR (Fig. S3 and Table S1†).

2.1.2 Hardener synthesis. 11-Mercapto-1-undecanol was synthesized as follows: 10-Undecen-1-ol (8 g, 47 mmol) was added to a dry flask with a stir bar. Thioacetic acid (3.6 g, 47 mmol) was added, and the mixture was purged with N_2 for 10 min. Benzoin (200 mg, 0.9 mmol) was then dissolved in methanol (0.25 mL) and added to the flask. The reaction was then exposed to UV light (355 nm) overnight and the resulting mixture was washed with cold DCM and then recrystallized with cold methanol to afford crude *S*-(11-hydroxyundecyl) ethanethioate. The thioester was then refluxed with sodium hydroxide (4 equivalence) in methanol for 12 hours. The reaction was then neutralized with 2 M HCl in ice and mixed with 200 mL of diethyl ether. The organic layer was separated, washed with 100 mL of brine, dried over magnesium sulfate, and filtered. The filtrate was concentrated and then freeze dried to afford 9.4 g of white powder to give 11-mercapto-1-undecanol.

Two different adhesive hardeners were synthesized using 11-mercapto-1-undecanol and two silanes. In a round bottom flask equipped with a stir bar, 11-mercapto-1-undecanol was added to dry DCM and stirred at 0 °C in an ice bath. Imidazole

(1 equiv.) was added, and the reaction was purged with nitrogen for 10 minutes. Then a silane (0.25 eq. for tetrachlorosilane and 0.5 eq. for dichlorodiisopropylsilane) was added dropwise and a white precipitate formed immediately. The reaction was allowed to warm to room temperature and reacted overnight. The solvent was then evaporated, and the remaining white precipitate was washed with ether and filtered. The ether solution was then dried leaving a yellow liquid. Purification by column chromatography on silica gel (15 : 1 hexane/ethyl acetate) provided a clear foul-smelling liquid.

2.1.3 Adhesive curing. Adhesives were formulated by mixing lignin and hardener together with appropriate weight ratios. Using TSE-25 (see definition in Table 1) as an example, 250 mg of lignin and 750 mg of TSE were mixed in ethyl acetate, sonicated, and vortexed to make a dispersion. The mixture was allowed to evaporate in the fume hood overnight leading to a viscous mixture. An even layer of adhesive was applied to a surface using a doctor blade and then another surface was placed on top of the layer. The substrates were clamped together using binder clips to enhance adhesive contact between the two substrates. The system was then cured at 110 °C overnight and then allowed to cool to room temperature.

2.1.4 Fourier transform infrared (FT-IR). FT-IR spectra of samples were recorded on a PerkinElmer spectrum 100 FTIR spectrometer using an attenuated total reflection (ATR) method. Absorption spectra were recorded at 4 cm^{-1} resolution and the signal averaged over 32 scans.

2.1.5 Differential scanning calorimetry (DSC). A differential scanning calorimeter (Hitachi 7020) was used to analyze thermal properties of thermosets. A sample (5–10 mg) was encapsulated in a 40 μL aluminum pan. The sample was submitted to heating from 25 to 200 °C with a heating rate of 10 °C min^{-1} under a nitrogen atmosphere.

2.1.6 Lap shear test. Substrates such as stainless steel 304, 5052 aluminum, glass, wood, carbon fiber, high-density polyethylene (HDPE), poly(vinyl chloride) (PVC), poly(methyl methacrylate) (PMMA), and poly(tetrafluoroethylene) (PTFE) were washed and sonicated with ethanol and then dried under vacuum for 48 hours. The substrates were then placed in a Diener zepto one plasma cleaner and cleaned under oxygen for 5 minutes (Fig. S4a–c†).

Adhesives were applied and cured as discussed in the above section. Lap shear test was performed according to ASTM D1002. The substrate dimensions were 101.6 × 25.4 × 2 mm with a shear area of 12.7 × 25.4 mm yielding the total surface area for adhesives at 322.6 mm^2. Single lap joint was performed in triplicate on a Zwick Z010 with a grip surface area at 645.2 mm^2 on each side. The average value was reported, and the error bar was determined by dividing the standard deviation over the square root number of measurement reported (Fig. S4d†).

Table 1 Adhesive compositions of lignin and thiol silyl ethers (DSE-*X* or TSE-*X*, where DSE and TSE respectively refer to dithiol silyl ether and tetrathiol silyl ether, and *X* is wt% of allyl lignin)

Adhesive code	Lignin, wt%	DSE, wt%	TSE, wt%
DSE-25	25	75	0
DSE-50	50	50	0
DSE-75	75	25	0
TSE-25	25	0	75
TSE-50	50	0	50
TSE-75	75	0	25

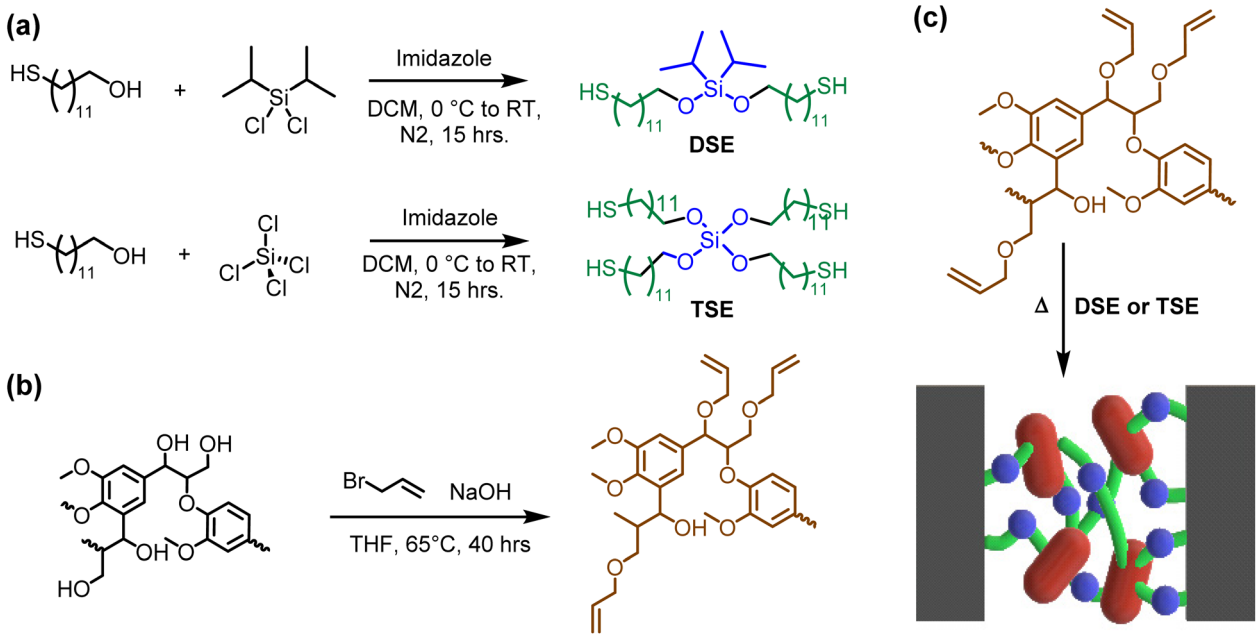

Scheme 1 (a) Synthesis of thiol silyl ethers; (b) synthesis of allyl lignin; (c) click chemistry between allyl lignin and thiol silyl ethers sandwiched between two substrates.

2.1.7 Rheology testing of resin. All rheological analyses were measured using a Discovery HR-2 (TA instruments, Delaware, USA) using a stainless-steel Peltier plate with a diameter of 40 mm. All rheological measurements were performed at 25 °C using a solvent trap to avoid evaporation during measurements. Oscillation frequency sweep measurements were performed at the shear strain of 1% with an angular frequency of 10 rad s^{-1}, duration of 300 s and a soak time of 180 s.

3. Results and discussion

3.1 Synthesis and curing of lignin based adhesives

Allyl lignin and disilyl crosslinkers, and tetrasilyl crosslinkers were prepared according to Scheme 1 according to a method previously reported.[33] Lignin was dissolved in THF and then allylated using allyl bromide under basic conditions. The reaction proceeded *via* Williamson ether substitution and was confirmed by NMR, the appearance of alkene protons in the range of δ 4.0–5.5 ppm, and by FTIR, a peak at 1550 cm^{-1} (Fig. S1 and S2†). The conversion of allylation was determined to be 85% *via* ^{31}P NMR (Table S1†). The hardeners were synthesized from silyl chlorides with high yields (>90%). Next the adhesive resins were formulated with different ratios of crosslinker to allyl lignin, which are listed in Table 1.

The adhesives were then cured at 120 °C in a vacuum oven to ensure the quantitative conversion of thiols and alkenes to thioethers. FTIR spectra show the strong peaks of Si–O and C–H bonds at 1086 cm^{-1} and 2920 cm^{-1} respectively, compared to the allylated lignin (Fig. 2a). DSC shows a broad peak starting at 140 °C, which is believed to originate from the curing reaction (Fig. 2b), somehow higher than those reported in literature.[35,36]

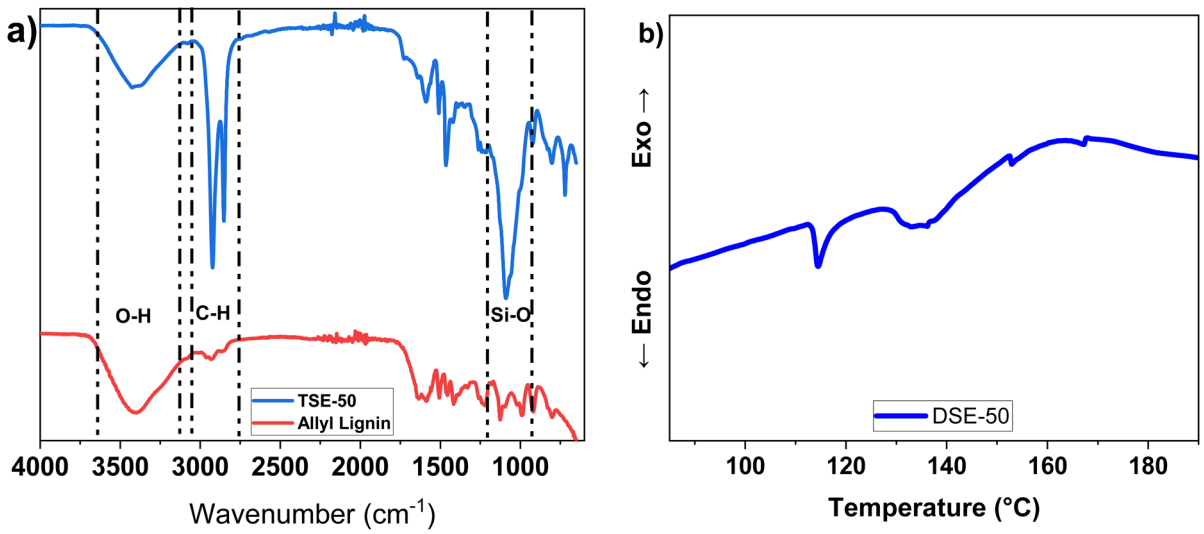

Fig. 2 Analysis of the curing behavior using DSE-50 an example: (a) FTIR spectra of allyl lignin and cured lignin; (b) DSC trace of curing of allyl lignin by DSE-50.

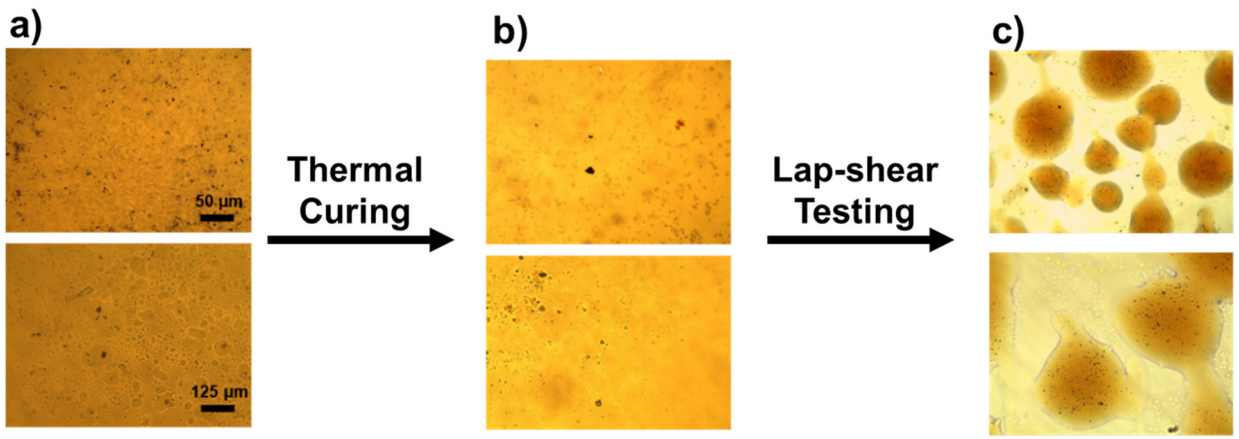

Fig. 3 Optical images of TSE-50 on glass plates: (a) before curing; (b) after curing; (c) after lap shear break.

Fig. 3 shows optical images of the adhesive applied, cured, and sheared. When the adhesive was deposited on the glass, a uniform layer was observed (Fig. 3a). After curing, no cracks or disruption in the adhesive layer were observed indicating the structural integrity was intact (Fig. 3b). After shear testing of the adhesive with the two glass plates separated, the failure mode was analyzed by examining the adhesive on the plates. Globular shapes of adhesive on both glass plates were observed (Fig. 3c), indicating cohesion is a possible failure mode.

3.2 Adhesion strength of lignin based adhesives

Several factors affect adhesion performance, including substrate surface energy, adhesive viscosity, and crosslinker chemistry.[37,38] To evaluate the effect of substrates on adhesion, nine different substrates were tested (Fig. 4), among which steel, wood, and glass generally performed the best. It is known that plasma cleaning can increase the polarity of steel surface and thus surface energy.[39–41] The increase in polarity, combined with the smoothness of surface, makes steel an

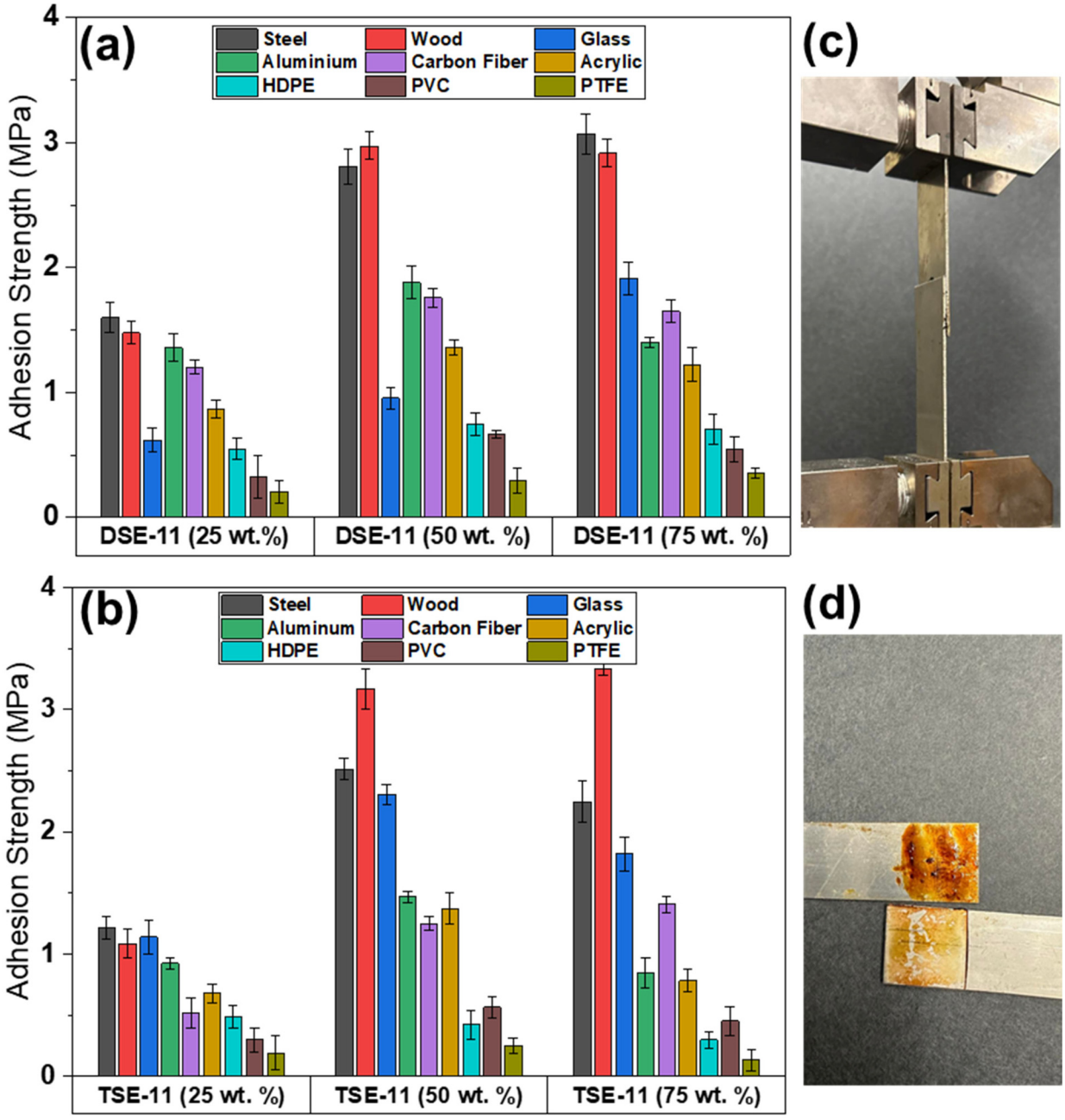

Fig. 4 Adhesion performance with different substrates by adhesives: (a) DSE and (b) TSE; optical images (c) before and (d) after lap-shear testing (use steel as an example).

ideal substrate for most adhesives. This can be seen with adhesion strength of over 2.0 MPa for many of the adhesives with lignin contents at 50 wt% and 75 wt%. A somewhat surprising observation was the performance of the adhesives on wood substrates. Since wood is uneven and porous, adhesive wetting of wood is often poor, leaving voids in the adhesive layer.[42] Despite this challenge, we observed the adhesion is comparable to or even better than that of steel. This could be due to the lignin presence in wood, which acts as a natural glue between cellulose and hemicellulose and may also offer good adhesion in lap-shear testing. Glass adhesion was also higher than expected since it typically possesses low surface energy. We rationalized this by examining the chemistry of the crosslinkers. Traditional glass adhesives contain either cyanoacrylates or silicone groups, which interact with the moisture on the glass surface.[43,44] The crosslinkers in this study contain siloxane units, which could promote improved compatibility and thus better adhesion between adhesives and glass surface.

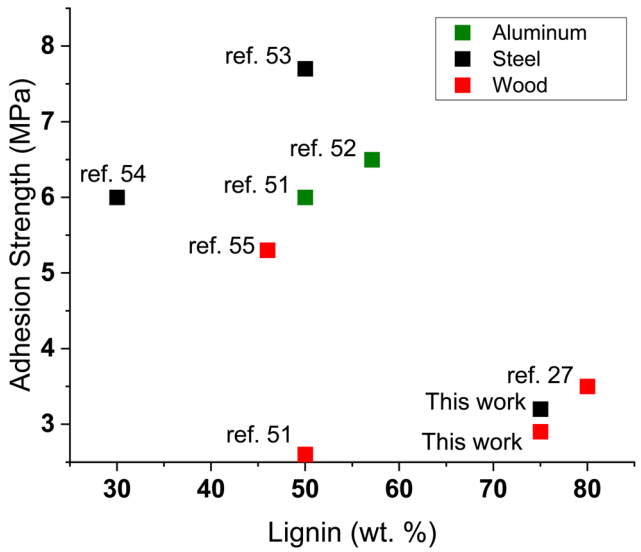

Fig. 5 Comparison of lignin-based adhesives and lignin wt% in literature.

Aluminum and carbon fiber displayed similar adhesion strength for each adhesive. Aluminum's oxide layer can often impair the adhesive layer. This minimizes the interactions between the adhesive and the substrate thus weakening the bond. Despite these hurdles, adhesion strength around 1.5 MPa was obtained for aluminum and carbon fiber when the lignin contents were 50 wt% and 75 wt%. Finally, the adhesion performance of organic polymer substrates was examined. With higher contents of lignin, the adhesives on acrylic or PMMA plastics exhibited the highest adhesion strength (1–1.5 MPa) due to the polarity of substrates, which allows for hydrogen bonding interactions with free thiol and hydroxyl groups on lignin with the carbonyl groups on PMMA. However, MD simulations indicate the nonbonding interactions are minimal (Fig. S5†), which would explain why the difference between acrylic and other polymers substrates is minimal. HDPE and PVC displayed similar adhesion across all adhesives. This is in line with our predictions as the nonpolar nature of HDPE is responsible for the lower surface energy. For PVC, the presence of plasticizers, which could migrate at the interface, may reduce adhesion strength.[45,46] Lastly, PTFE possesses the lowest surface energy due to its inert C–F bonds that restrict interactions between the adhesive and the polymer. Unsurprisingly, PTFE gave the lowest adhesion strength, less than 0.5 MPa.

For DSE-25 and TSE-25, lower adhesion strength was observed for all substrates. This was attributed to the presence of excess thiols, which could induce a plasticizing effect that would lead to weaker adhesion.[33,47] Once the free thiol content is reduced, the plasticizing effect is greatly reduced, making the adhesives stronger with higher lignin contents.[48–50]

The adhesion performance of these adhesives was then compared to other lignin-based adhesives reported in

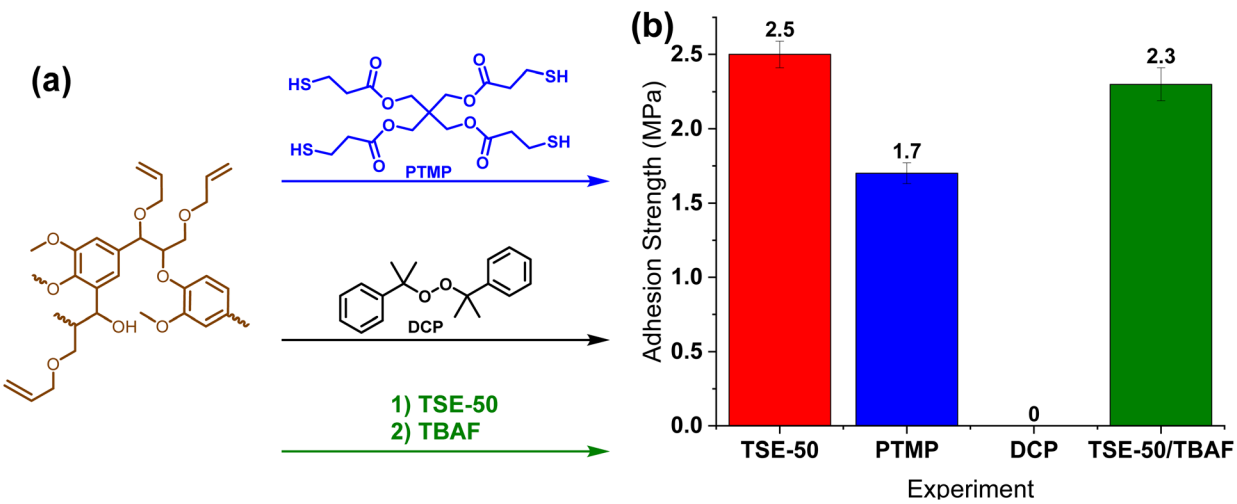

Fig. 6 (a) Mechanistic experiments studying adhesion on steel plates with non-silicone containing tetrathiol crosslinker (PTMP); peroxide crosslinker (DCP); with TSE and then immersed in TBAF; (b) adhesion strength of neat TSE-50 and the above treated TSE-50.

literature.[27,51–57] The results are presented in Fig. 5. The adhesives developed in this work show lower adhesion strength but incorporate a higher biomass content. Compared to other reported adhesives that incorporate a higher lignin fraction (>60 wt%), a similar adhesion performance is achieved.

3.3 Mechanisms of adhesion

The adhesion mechanism was then explored. Fig. 6a shows the experiments to determine what effect each reaction component has on the adhesives. First, raw lignin was crosslinked with dicumyl peroxide (DCP) to create a thermoset network between two plates. However, upon curing no adhesion was observed. Raw lignin is brittle and mechanically weak, so it was not surprising that just crosslinked lignin was insufficient for adhesion, instead a crosslinker had to be used.[58] Next, the effect of silyl ethers was evaluated through two experiments. Pentaerythritol tetrakis(3-mercaptopropionate) (PTMP) was chosen due to its tetra functionality and similarity to TSE. As shown in Fig. 6b, with lignin at 50 wt%, adhesion strength on steel plates was observed to be 1.7 MPa, significantly lower than 2.5 MPa for TSE-50. This result suggested that the silyl ether enhances the adhesion most likely due to nonbonding interactions with the surface. To further investigate this claim, TSE-50 was immersed in 1 M tetra-*n*-butylammonium fluoride (TBAF) in THF overnight to cleave Si–O bonds. A minor reduction in adhesion strength was observed (Fig. 6b), indicating that either the adhesive seal was too strong to degrade or the resulting alcohols from the silyl ether cleavage may also participate in the adhesion process.

Many adhesives fail to bond wooden substrates due to their porous surfaces.[59,60] One important factor is the ability of adhesives to maintain contact with the wood surfaces without being absorbed into the substrate. Given the high adhesion on wood substrates, the rheology of TSE-50 adhesive resin at room temperature was studied (Fig. 7).

The TSE-50 resin displays highly viscous behavior even at higher frequencies. The high viscosity is advantageous when the adhesive is applied to wood surfaces, which are typically not smooth. During the curing process adhesives may be absorbed into the wooden pores thus lowering the wettability

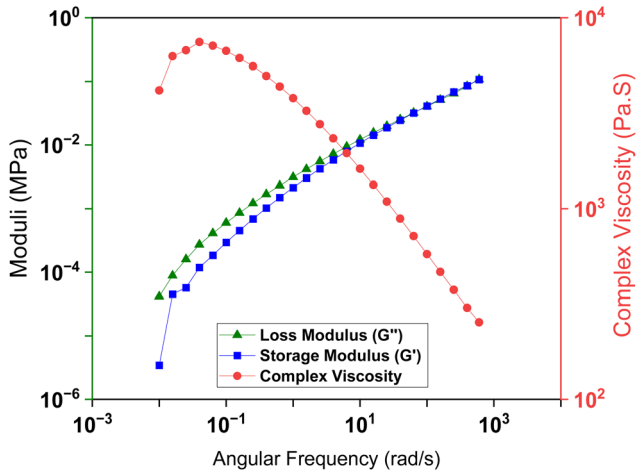

Fig. 7 Rheological plots of TSE-50 before curing.

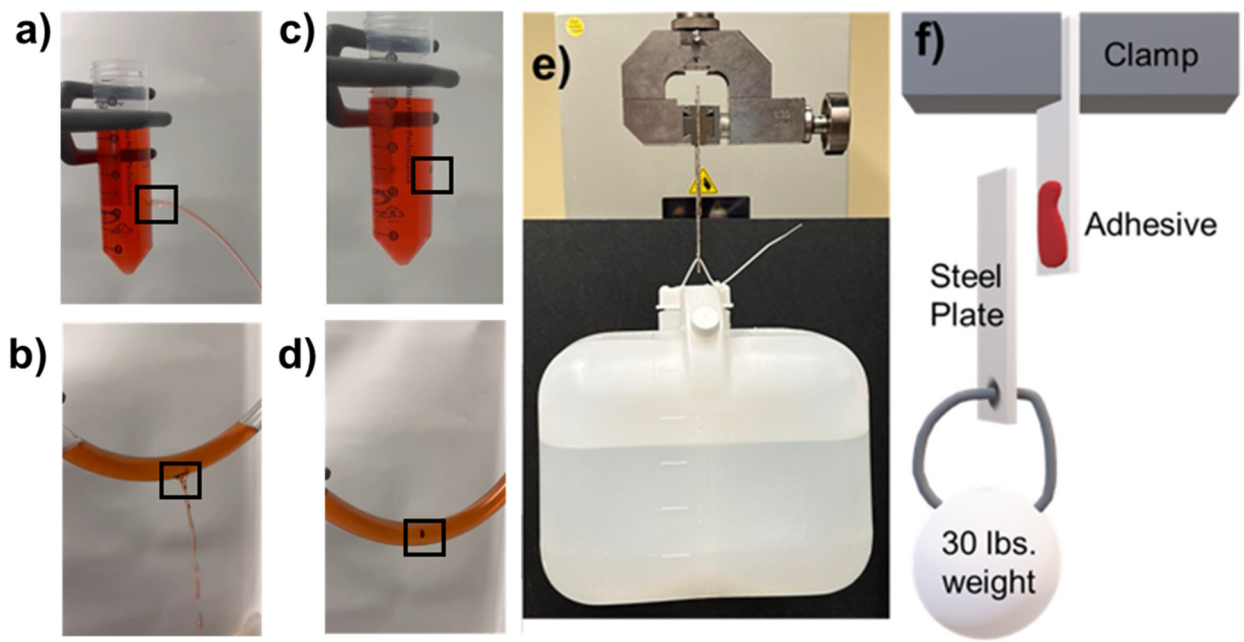

Fig. 8 Optical graphs of TSE-50 testing as an adhesive: (a) unrepaired rigid polypropylene centrifuge tube with a leak; (b) flexible polyvinyl chloride Tygon® tubing with a leak; (c) repaired rigid polypropylene centrifuge tube; (d) repaired flexible polyvinyl chloride Tygon® tubing; (e) optical graphs of adhesive under a prolonged load; (f) schematic representation of the prolonged load test.

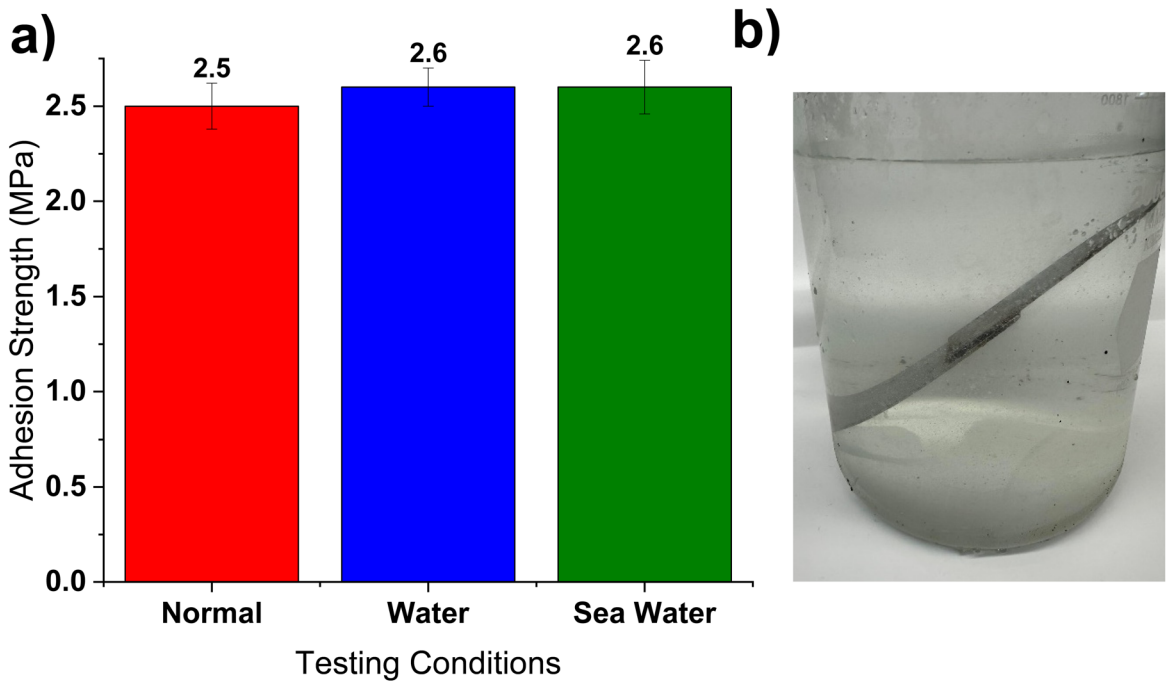

Fig. 9 Adhesion performance of TSE-50 under dry and wet conditions. (a) Lap shear results under different environments (exposed to air and immersed in water or sea water for 21 days); (b) optical image of two steel plates adhered by TSE-50 under water.

and the adhesion.[61] In the case of this viscous adhesive an even layer of TSE-50 is present and is not absorbed into the wooden substrate which maximizes the adhesion surface area.

The adhesion mechanism was also explored by molecular dynamics simulations by modeling the interface between lignin and cellulose (representing the wood substrate) (see ESI†). The simulations only studied nonbonding interactions including the van der Waals and electrostatic interactions. Although the lack of covalent bonding interactions in the simulations, the interfacial energy between raw lignin and cellulose was calculated (Fig. S5†) to be (100 ± 9) mJ m^{-2}, which agrees with a recent study of lignin-cellulose interfaces.[62]

3.4 Adhesion applications

The TSE-50 adhesive was selected for testing its application by applying it to flexible and rigid plastics. When exposed to flow the adhesive acted as a plug to block the leakage of liquid, as shown in Fig. 8a–d. This further indicated its efficacy as an adhesive and demonstrated the adhesive's water resistance. Fig. 8e and f also demonstrates TSE-50 ability to withstand loads at a prolonged time. Even after 21 days the adhesive was able to maintain its adhesion.

The TSE-50 adhesive was then tested in aqueous conditions to determine what effect if any wet environments had on the adhesion strength (Fig. 9). Two TSE-50 samples were prepared by sandwiching the adhesive between steel substrates. One sample was submerged in distilled water and the other sample was submerged in 3 wt% NaCl in water mimicking the composition of seawater.[63] Both samples were submerged for 21 days and then the adhesion force was recorded. The adhesion strength did not change regardless of testing conditions. This isn't too surprising since the adhesive crosslinked with non-hydrolysable bonds. This result further supported the observations from Fig. 8, indicating the durability of this adhesive underwater.

4. Conclusions

Lignin-based adhesives using thiol–silyl ether crosslinkers were prepared with high biomass contents. The adhesives show a broad spectrum of adhesion across a wide range of polar substrates. The adhesion mechanism was explored using different crosslinkers to shed light on interfacial molecular interactions. The liquid leakage and load bearing experiments demonstrated the potential of this class of adhesives as sustainable green materials for real-world applications.

Conflicts of interest

There are no conflicts to declare.

Acknowledgements

The support from the U.S. National Science Foundation (DMR1806792) is acknowledged. The authors would like to acknowledge Caroline Rohlfing for her help in the lap-shear testing of the adhesives.

References

1 M. A. R. Lubis, F. P. Sari, R. P. B. Laksana, W. Fatriasari and E. Hermiati, *Polym. Bull.*, 2022, **79**, 6745–6757.
2 Z. Heng, Y. Chen, H. Zou and M. Liang, *RSC Adv.*, 2015, **5**, 42362–42368.
3 F.-L. Jin, X. Li and S.-J. Park, *J. Ind. Eng. Chem.*, 2015, **29**, 1–11.
4 L. A. Heinrich, *Green Chem.*, 2019, **21**, 1866–1888.
5 J. E. McDevitt and W. J. Grigsby, *J. Polym. Environ.*, 2014, **22**, 537–544.
6 Y. Hu, Z. Kou, Y. Ma, Q. Huang, Y. Sha, M. Zhang, L. Hu, P. Jia and Y. Zhou, *ACS Sustainable Chem. Eng.*, 2023, **11**, 13492–13501.
7 M. S. Ganewatta, Z. Wang and C. Tang, *Nat. Rev. Chem.*, 2021, **5**, 753–772.
8 L. Yuan, L. B. Kurnaz and C. Tang, *Nat. Sustain.*, 2021, **4**, 837–838.
9 J. Wang, K. Yao, A. L. Korich, S. Li, S. Ma, H. J. Ploehn, P. M. Iovine, C. Wang, F. Chu and C. Tang, *J. Polym. Sci., Part A: Polym. Chem.*, 2011, **49**, 3728–3738.
10 Z. Wang, M. S. Ganewatta and C. Tang, *Prog. Polym. Sci.*, 2020, **101**, 101197.
11 L. B. Kurnaz, Y. Bension and C. Tang, *Macromol. Chem. Phys.*, 2022, **224**, 2200303.
12 S. Bertella and J. S. Luterbacher, *Trends Chem.*, 2020, **2**, 440–453.
13 J. Hwang, D. V. Martinez, E. J. Martinez, G. Metavarayuth, D. Goodlett, Q. Wang, M. Ganewatta, M. S. Kent and C. Tang, *Giant*, 2022, **10**, 100106.
14 L. Yuan, Y. Zhang, Z. Wang, Y. Han and C. Tang, *ACS Sustainable Chem. Eng.*, 2019, **7**, 2593–2601.
15 J. Yu, J. Wang, C. Wang, Y. Liu, Y. Xu, C. Tang and F. Chu, *Macromol. Rapid Commun.*, 2015, **36**, 398–404.
16 Y. Xu, L. Yuan, Z. Wang, P. A. Wilbon, C. Wang, F. Chu and C. Tang, *Green Chem.*, 2016, **18**, 4974–4981.
17 J. Ruwoldt, F. H. Blindheim and G. Chinga-Carrasco, *RSC Adv.*, 2023, **13**, 12529–12553.
18 M. Osaki, T. Sekine, H. Yamaguchi, Y. Takashima and A. Harada, *ACS Appl. Polym. Mater.*, 2021, **3**, 2189–2196.
19 C. Cui and W. Liu, *Prog. Polym. Sci.*, 2021, **116**, 101388.
20 J. Steck, J. Yang and Z. Suo, *ACS Macro Lett.*, 2019, **8**, 754–758.
21 T. Lin, Y. Wu, E. Santos, X. Chen, J. Kelleher-Ferguson, C. Tucker, D. Ahn, C. Mohler and Z. Chen, *Langmuir*, 2022, **38**, 2590–2600.
22 Y. Liang, K. Wang, J. Li, Y. Zhang, J. Liu, K. Zhang, Y. Cui, M. Wang and C.-S. Liu, *Mater. Horiz.*, 2022, **9**, 1700–1707.
23 S. Yang, J. Bai, X. Sun and J. Zhang, *Chem. Eng. J.*, 2023, **461**, 142066.
24 S.-X. Hou, J. Zhang, G. Wu, S.-C. Chen and Y.-Z. Wang, *ACS Sustainable Chem. Eng.*, 2023, **11**, 10667–10676.
25 D. E. Packham, *Int. J. Adhes. Adhes.*, 2003, **23**, 437–448.
26 Z. Wang, L. Yuan and C. Tang, *Acc. Chem. Res.*, 2017, **50**, 1762–1773.
27 M. Siahkamari, S. Emmanuel, D. B. Hodge and M. Nejad, *ACS Sustainable Chem. Eng.*, 2022, **10**, 3430–3441.
28 A. F. Ang, Z. Ashaari, S. H. Lee, P. Md Tahir and R. Halis, *Int. J. Adhes. Adhes.*, 2019, **95**, 1879–0127.
29 M. H. Hussin, N. H. Abd Latif, T. S. Hamidon, N. N. Idris, R. Hashim, J. N. Appaturi, N. Brosse, I. Ziegler-Devin, L. Chrusiel, W. Fatriasari, F. A. Syamani, A. H. Iswanto, L. S. Hua, S. S. A. O. Al Edrus, W. C. Lum, P. Antov, V. Savov, M. A. Rahandi Lubis, L. Kristak, R. Reh and J. Sedliačik, *J. Mater. Res. Technol.*, 2022, **21**, 3909–3946.
30 M. A. Jedrzejczyk, P. D. Kouris, M. D. Boot, E. J. M. Hensen and K. V. Bernaerts, *ACS Appl. Polym. Mater.*, 2022, **4**, 2544–2552.
31 M. Jia, A. Li, Y. Mu, W. Jiang and X. Wan, *Polymer*, 2014, **55**, 1160–1166.
32 A. Tarafdar, R. Sirohi, P. A. Balakumaran, R. Reshmy, A. Madhavan, R. Sindhu, P. Binod, Y. Kumar, D. Kumar and S. J. Sim, *J. Hazard. Mater.*, 2022, **423**, 127097.
33 Y. Bension, L. B. Kurnaz, T. Ge and C. Tang, *Macromolecules*, 2023, **56**, 2831–2840.
34 M. Jawerth, M. Johansson, S. Lundmark, C. Gioia and M. Lawoko, *ACS Sustainable Chem. Eng.*, 2017, **5**, 10918–10925.
35 D. Guzmán, X. Ramis, X. Fernández-Francos and A. Serra, *RSC Adv.*, 2015, **5**, 101623–101633.
36 W. D. Cook, F. Chen, D. W. Pattison, P. Hopson and M. Beaujon, *Polym. Int.*, 2007, **56**, 1572–1579.
37 J. R. Huntsberger, *J. Adhes.*, 1981, **12**, 3–12.
38 J. D. Valentin, X.-H. Qin, C. Fessele, H. Straub, H. C. van der Mei, M. T. Buhmann, K. Maniura-Weber and Q. Ren, *J. Colloid Interface Sci.*, 2019, **552**, 247–257.
39 M. Frascio, C. Mandolfino, F. Moroni, M. Jilich, A. Lagazzo, M. Pizzorni, L. Bergonzi, C. Morano, M. Alfano and M. Avalle, *Int. J. Adhes. Adhes.*, 2021, **106**, 102802.
40 D. Marinov, J.-F. de Marneffe, Q. Smets, G. Arutchelvan, K. M. Bal, E. Voronina, T. Rakhimova, Y. Mankelevich, S. El Kazzi and A. Nalin Mehta, *npj 2D Mater. Appl.*, 2021, **5**, 17.
41 M. Berczeli and Z. Weltsch, *Polymers*, 2021, **13**, 901.
42 M. Dunky, *Progress in Adhesion and Adhesives*, 2021, vol. 6, pp. 761–840.
43 J. Thiemecke and R. Hensel, *Adv. Funct. Mater.*, 2020, **30**, 2005826.
44 O. Fifo, K. Ryan and B. Basu, *J. Compos. Mater.*, 2014, **48**, 2657–2668.
45 M. Aznar, P. Vera, E. Canellas, C. Nerín, P. Mercea and A. Störmer, *J. Mater. Chem.*, 2011, **21**, 4358–4370.
46 X. Zhang, Y. Li, J. M. Hankett and Z. Chen, *Phys. Chem. Chem. Phys.*, 2015, **17**, 4472–4482.
47 Y. Jin, X. Cheng and Z. Zheng, *Bioresour. Technol.*, 2010, **101**, 2046–2048.
48 H. Yang, X. Tan, G. Du, K. Ni, Y. Wu, Z. Li, X. Ran, W. Gao, J. Li and L. Yang, *Composites, Part B*, 2023, **263**, 110872.
49 C. Gu, M. R. Dubay, S. J. Severtson and L. E. Gwin, *Ind. Eng. Chem. Res.*, 2014, **53**, 11000–11006.
50 G. Xiao, J. Liang, Z. Wu, H. Lei, F. Gong, W. Gu, Y. Tu and D. Li, *Forests*, 2023, **14**, 1250.

51 A. Moreno, M. Morsali and M. H. Sipponen, *ACS Appl. Mater. Interfaces*, 2021, **13**, 57952–57961.
52 S. Zhang, T. Liu, C. Hao, L. Wang, J. Han, H. Liu and J. Zhang, *Green Chem.*, 2018, **20**, 2995–3000.
53 F. Ferdosian, Y. Zhang, Z. Yuan, M. Anderson and C. Xu, *Eur. Polym. J.*, 2016, **82**, 153–165.
54 J. R. Gouveia, G. E. S. Garcia, L. D. Antonino, L. B. Tavares and D. J. dos Santos, *Molecules*, 2020, **25**, 2513.
55 F. R. Vieira, N. Gama, S. Magina, A. Barros-Timmons, D. V. Evtuguin and P. C. O. R. Pinto, *Polymers*, 2022, **14**, 5305.
56 G. Yang, Z. Gong, X. Luo, L. Chen and L. Shuai, *Nature*, 2023, **621**, 511–515.
57 R. J. Li, J. Gutierrez, Y.-L. Chung, C. W. Frank, S. L. Billington and E. S. Sattely, *Green Chem.*, 2018, **20**, 1459–1466.
58 C. Huang, Z. Peng, J. Li, X. Li, X. Jiang and Y. Dong, *Ind. Crops Prod.*, 2022, **187**, 115388.
59 F. Simon and G. Valentin, in *European Structural Integrity Society*, ed. B. R. K. Blackman, A. Pavan and J. G. Williams, Elsevier, 2003, vol. 32, pp. 305–316.
60 R. M. Rowell, *Polymers*, 2021, **13**, 2558.
61 Y. Wang, C. J. Hansen, C.-C. Wu, E. J. Robinette and A. M. Peterson, *RSC Adv.*, 2021, **11**, 31142–31151.
62 S. Youssefian and N. Rahbar, *Sci. Rep.*, 2015, **5**, 11116.
63 D. H. Heinrich, *Am. J. Sci.*, 2005, **305**, 220–239.